SHRIMP-RG U-Pb isotopic systematics of zircon from the Angel Lake orthogneiss, East Humboldt Range, Nevada: Is this really Archean crust?

Wayne R. Premo
U.S. Geological Survey, MS 963, Box 25046, Denver Federal Center, Denver, Colorado 80225, USA

Pedro Castiñeiras
Departamento de Petrología y Geoquímica, Universidad Complutense de Madrid, c/ José Antonio Novais 2, Madrid 28040, Spain

Joseph L. Wooden
U.S. Geological Survey, 345 Middlefield Road, Menlo Park, California 94025, USA

ABSTRACT

New SHRIMP-RG (sensitive high-resolution ion microprobe–reverse geometry) data confirm the existence of Archean components within zircon grains of a sample from the orthogneiss of Angel Lake, Nevada, United States, previously interpreted as a nappe of Archean crust. However, the combined evidence strongly suggests that this orthogneiss is a highly deformed, Late Cretaceous monzogranite derived from melting of a sedimentary source dominated by Archean detritus. Zircon grains from the same sample used previously for isotope dilution–thermal ionization mass spectrometry (ID-TIMS) isotopic work were analyzed using the SHRIMP-RG to better define the age and origin of the orthogneiss. Prior to analysis, imaging revealed a morphological variability and intragrain, polyphase nature of the zircon population. The SHRIMP-RG yielded $^{207}Pb/^{206}Pb$ ages between ca. 2430 and 2580 Ma (a best-fit mean $^{207}Pb/^{206}Pb$ age of 2531 ± 19 Ma; 95% confidence) from mostly rounded to subrounded zircons and zircon components (cores). In addition, several analyses from rounded to subrounded cores or grains yielded discordant $^{207}Pb/^{206}Pb$ ages between ca. 1460 and ca. 2170 Ma, consistent with known regional magmatic events.

All cores of Proterozoic to latest Archean age were encased within clear, typically low Th/U (<0.015), oscillatory zoned, mostly euhedral, Late Cretaceous zircon. The younger zircon yielded essentially concordant $^{206}Pb/^{238}U$ ages between 72 and 91 Ma, consistent with magmatic ages from Lamoille Canyon to the south. An age of ca. 90 Ma is suggested, the younger $^{206}Pb/^{238}U$ ages resulting from Pb loss. The Cretaceous and Precambrian zircon components also have distinct trace element characteristics, indicating that these age groups are not related to the same igneous source.

These results support recent geophysical interpretations and negate the contention that the Archean-Proterozoic boundary extends into the central Great Basin area. They further suggest that the world-class gold deposits along the Carlin Trend are not underlain by Archean cratonal crust, but rather by the Proterozoic Mojave province and Neoproterozoic and Paleozoic metasedimentary sequences dominated by detritus derived from Late Archean sources rather than Proterozoic sources, as is evident farther to the south in the Ruby Mountains.

INTRODUCTION

The Ruby Mountains and their northern extension, the East Humboldt Range, of northeastern Nevada, United States (Fig. 1) are the result of Late Cretaceous to mid-Tertiary core complex formation and Basin and Range extensional tectonism that is active today (Howard, 1966, 2003; Howard et al., 1979; Snoke et al., 1997). In these ranges, contrasting migmatitic, mid-crustal level basements form the core complex infrastructure. To the north, Precambrian and early Paleozoic metamorphic rocks are deformed, metamorphosed, and intruded by several generations of Late Cretaceous to Eocene plutonic rocks. To the south, Neoproterozoic to Late Devonian strata form the infrastructure for essentially the same suite of plutonic rocks. The plutonic rocks range from gabbro (although very minor) to pervasive swarms of two-mica monzogranite and leucogranite, often containing abundant muscovite, sillimanite, garnet, and monazite. Several quartz dioritic to granodioritic bodies are exposed in both the northern (East Humboldt Range) and southern (Ruby Mountains) ranges. New U-Pb SHRIMP (sensitive high-resolution ion microprobe) ages identify four pulses of magmatism within the Ruby Mountains–East Humboldt Range during the Late Jurassic (ca. 155 Ma), early Late Cretaceous (ca. 90 Ma), Late Cretaceous (ca. 69 Ma), and Eocene–Oligocene (ca. 40–29 Ma).

Previously, workers have proposed the existence of Archean crust in the core of a nappe in the Angel Lake area of the northern East Humboldt Range (Lush et al., 1988), based on a U-Pb zircon age of 2520 ± 110 Ma for the orthogneiss of Angel Lake (sample RM-9, collected by Jim Wright). However, this age was obtained using the isotope dilution–thermal ionization mass spectrometry (ID-TIMS) method on five multi-milligram size fractions that yielded very discordant results, leading to a significant uncertainty in the reported age. Petrographic analysis of the zircon populations revealed abundant inherited cores, interpreted by Lush et al. (1988) as one of the major causes of discordance. High uranium concentrations in the zircons (1000–2500 ppm) further increased the likelihood of lead (Pb) loss.

It is important to establish an accurate age for this piece of proposed Archean crust to ascertain the true extent of Archean cratonic crust in the subsurface southwestward from exposures in Wyoming. Some past studies proposed that the Archean extends as far west as northeastern Nevada, generally near the Carlin Trend (e.g., DePaolo and Farmer, 1984; Bennett and DePaolo, 1987; Wright and Wooden, 1991; Tosdal et al., 2003; Mueller and Frost, 2006). Recent studies have questioned the existence of Archean

Geosphere; December 2008; v. 4; no. 6; p. 963–975; doi: 10.1130/GES00164.1; 9 figures; 2 tables.

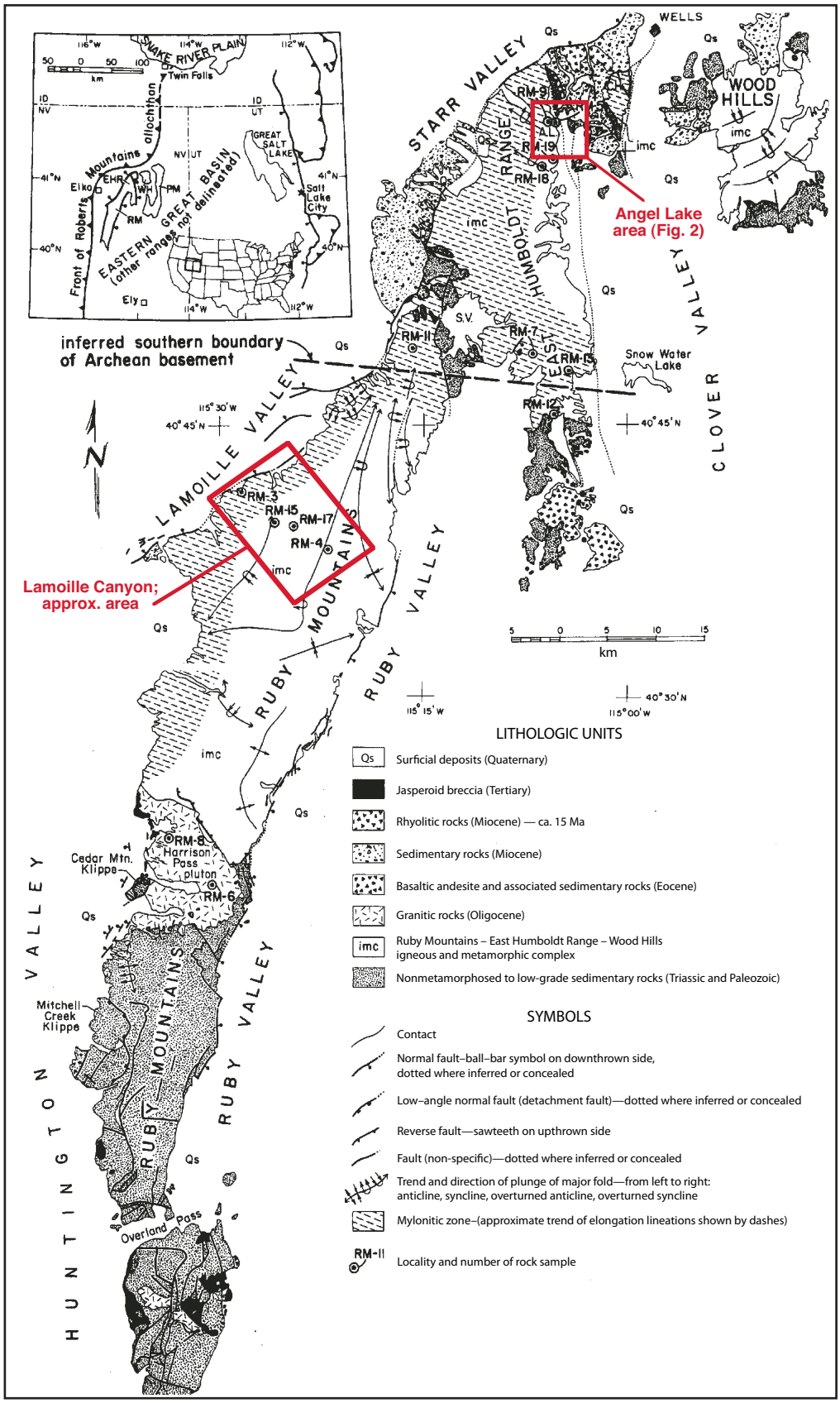

Figure 1. Generalized geologic map of the East Humboldt Range (EHR), Wood Hills (WH), and Ruby Mountains (RM), Nevada, showing the approximate location of RM-9, the analyzed rock sample. A.L.—Angel Lake; S.V.—Secret Valley. The inset map shows the locations of RM, EHR, WH, and Pequop Mountains (PM) with respect to large-scale tectonic features in the region (after Snoke et al., 1990; Wright and Snoke, 1993).

crust at preestablished exposures in the Farmington Canyon Complex near Salt Lake City (Nelson et al., 2002; Stroud et al., 2007). However, most investigators agree that Archean rocks are exposed in the Grouse Creek–Albion–Raft River Ranges of northwestern Utah–southern Idaho (Egger et al., 2003). The distribution of Archean crust has important implications for gold metallogeny in the Great Basin because such rocks can be auriferous (e.g., Cameron, 1988).

Determination of the age(s) of zircon population(s) in the Angel Lake orthogneiss may aid in identifying whether the Winchell Lake nappe is indigenous to Laurentia, possibly linking it to an existing regional province (e.g., the Wyoming Province), or whether it is related to some other Archean craton, now rifted away, or something else. The answer has important implications for tectonic models regarding the crustal evolution of the southwestern margin of North America.

One method that is often employed to investigate complex zircons is the SHRIMP, which uses a small beam (~10–35 mm in diameter) to measure the U-Pb isotopic systematics within highly localized and reasonably well defined areas of the zircon crystal (e.g., Davis et al., 2003). Thus, areas of inheritance and Pb loss can be identified.

GEOLOGY

The Ruby Mountains–East Humboldt Range uplifts, located in northeastern Nevada (Fig. 1), together form one of many North American Cordilleran metamorphic core complexes (Crittenden et al., 1980; Howard, 2000), and by definition expose middle-crustal metamorphic rocks as a result of extensional, low-angle, normal faulting. In many cases, the low-angle faulting is plastic to brittle in nature, and well-developed mylonites are common.

The pre-Quaternary rocks of the Ruby Mountains–East Humboldt Range can be divided into the following generalized groups: (1) nonmetamorphosed to low-grade Triassic, Paleozoic, and Neoproterozoic miogeoclinal rocks, (2) an igneous-metamorphic and migmatitic complex composed of mostly upper amphibolite-grade metasedimentary rocks intruded by late Mesozoic–Tertiary granitic rocks, (3) Eocene granitic plutons, (4) broad zones of mylonitic to submylonitic rocks involving all of the above groups to some degree, and (5) Tertiary volcanic and sedimentary rocks (Snoke et al., 1990; Wright and Snoke, 1993; Fig. 1). In the northern Ruby Mountains and East Humboldt Range, Late Cretaceous crustal shortening, metamorphism, and magmatism are evidenced by an early thrust system, the development of fold nappes, widespread migmatization, injection of monzogranitic and leucogranitic magmas, and accompanying sillimanite-grade metamorphism (Snoke et al., 1997). This contractional tectonism was followed by a protracted, Late Cretaceous–Eocene, extensional deformation, followed by late Eocene–Oligocene monzogranitic to leucogranitic magmatism, and the formation of a west-directed, extensional shear zone responsible for Oligocene–Miocene core complex exhumation (Snoke et al., 1997). More detailed geologic descriptions and explanations can be found in Sharp (1942), Howard (1966, 1980, 2003), Wright and Snoke (1993), and Snoke et al. (1997).

Angel Lake Area

Rocks interpreted as Archean basement are exposed in the core of a large-scale recumbent fold called the Winchell Lake nappe in the Angel Lake area of the East Humboldt Range, and include orthogneiss, paragneiss, and amphibolite—the metamorphic suite of Angel Lake (Lush et al., 1988; Fig. 2). The orthogneiss is highly deformed and K-feldspar porphyroclasts are locally common. The paragneiss was once a heterogeneous siliciclastic sedimentary sequence, but now consists of pure to impure quartzite and psammitic to pelitic schist, and is highly deformed (Lush et al., 1988). Late Proterozoic–Cambrian impure quartzite and schist, and early Paleozoic dolomitic and calcitic marble, quartzite, and calc-silicate rocks, also crop out in the Angel Lake area. Deformed and metamorphosed hornblende-biotite quartz diorite to monzogranite (now orthogneiss) intruded much of the Paleozoic section (Fig. 2).

PREVIOUS GEOCHRONOLOGY

Zircons from the orthogneiss of Angel Lake were previously analyzed using ID-TIMS methodology. The interpretation based on analysis of five multi-milligram size fractions was an Archean concordia upper-intercept age of 2520 ± 110 Ma and accompanying lower-intercept age of 196 ± 32 Ma (Lush et al., 1988). The U-Pb results are, however, very discordant (~50% and greater). Lush et al. (1988) acknowledged that the isotopic data could be interpreted to suggest a Mesozoic emplacement age for the orthogneiss, with an older inherited Archean zircon component.

Other dates from samples of the East Humboldt Range include U-Pb monazite and zircon ages between ca. 85 and 29 Ma for quartz dioritic to monzogranitic orthogneisses that were interpreted as crystallization ages (Wright and Snoke, 1993). Most of these bodies occur as sills or dike-like intrusions (Lush, 1982; McGrew, 1992; Wright and Snoke, 1993). A syntectonic leucogranite from the hinge zone of the large-scale recumbent fold of the Winchell Lake nappe yielded a mean $^{207}Pb/^{206}Pb$ age of 84.8 ± 2.8 Ma (McGrew et al., 2000) on zircon. Samples of quartz dioritic and granodioritic orthogneiss yielded U-Pb zircon concordia lower-intercept ages of 40 ± 3 and 35 ± 3 Ma, respectively, with an average age of inheritance suggested to be 2390 ± 40 Ma (Wright and Snoke, 1993). In addition, quartz dioritic dikes yielded U-Pb zircon ages of 38 ± 2 Ma (concordia lower intercept; Wright and Snoke, 1993) and 39 ± 0.5 Ma (SHRIMP; Premo, 2008, personal observ.), and initial εNd values of −16.5 and −17.0, respectively. Xenocrystic zircon within some grains from the former sample yielded an ill-defined upper-intercept age of ca. 2300 Ma. U-Pb ages for monzogranitic orthogneiss ranged from ca. 32 Ma (zircon) to 29 ± 0.5 Ma (monazite) with initial εNd values of −24.5 and −25, and an average age of 2430 ± 40 Ma for a premagmatic zircon component (Wright and Snoke, 1993).

ANALYTICAL METHODS

SHRIMP procedures used in this study are similar to those reported in Williams (1997). Zircons handpicked from the same population separated for ID-TIMS work and chips of zircon standard R33 were mounted in epoxy, ground to nearly half their thickness using 1500 grit, wet-dry sandpaper, and polished with 6 and 1 mm grit diamond suspension abrasive. Transmitted- and reflected-light photos were taken of all mounted grains. In addition, cathodoluminescence (CL) images of all zircons were prepared prior to analysis and used to reveal internal zoning related to chemical composition in order to avoid possible problematic areas within grains. The mounts were cleaned in 1N HCl and gold coated for maximum surface conductivity. The U-Th-Pb analyses were made using the SHRIMP-RG (reverse geometry) housed in Green Hall at Stanford University, California, and co-owned by the U.S. Geological Survey. The primary oxygen ion beam operated at ~4–6 nA and excavated an area of ~25–35 μm in diameter to a depth of ~1 μm. Data for each spot were collected in sets of six scans through the mass range. The reduced $^{206}Pb/^{238}U$ ratios were normalized to zircon standard R33 (monzodiorite, Braintree Complex, Vermont; 419 Ma, Black et al., 2004) and CZ3 (550 ppm U; Pidgeon et al., 1994); these standard values are based on conventional U-Pb dating of replicate isotope dilution analyses of milligram-sized fragments. Analyses of samples

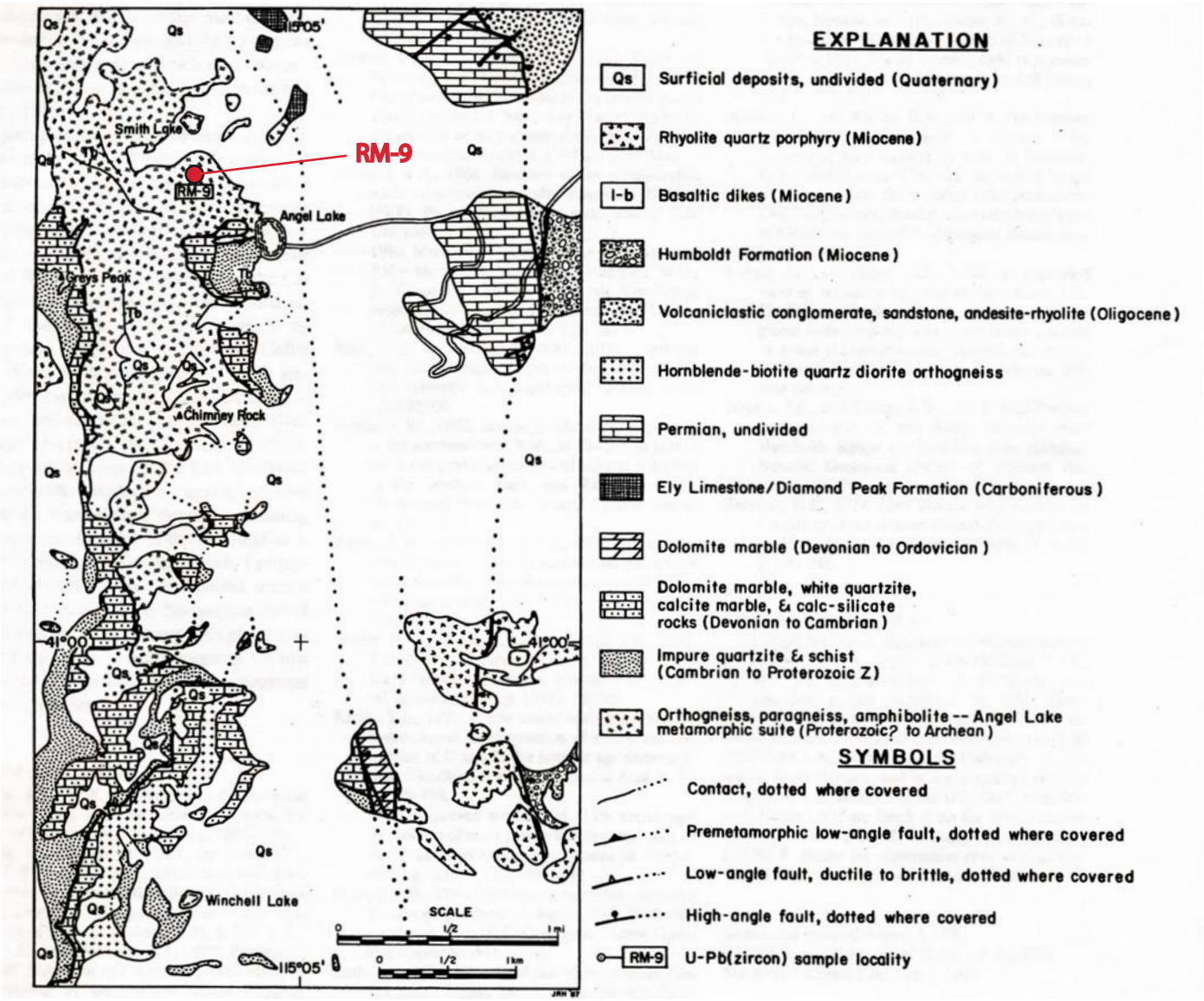

Figure 2. Generalized geologic map of a portion of the northern East Humboldt Range, modified from Lush (1982) and A.J. McGrew and A.W. Snoke (unpub. mapping). RM-9 indicates locality of analyzed orthogneiss sample (after Lush et al., 1988).

and standard were alternated for the closest control of Pb/U ratios. U, Th, and Pb concentrations are reproducible on the gem-quality standard at ~10% (2σ) and include real heterogeneity in the standard. Age-data reduction follows the methods described by Williams (1997) and Ireland and Williams (2003), and SQUID (version 1.08) and ISOPLOT (version 3.00) software (Ludwig, 2002, 2003) were used.

La to Yb and Hf were measured at the same time as the U-Th-Pb analyses as additional masses on each pass through the mass range. La to Yb and Hf concentrations are calibrated against CZ3 and are reproducible at 2%–4% (1σ), except for La (15%) because of its typical very low concentration (30 ppb). Absolute concentrations of CZ3 were derived by doping synthetic zircons with concentrations high enough to be measured by the electron microprobe and comparing these synthetic zircons to CZ3 on the ion microprobe.

SHRIMP-RG, U-Pb ZIRCON GEOCHRONLOGY

Zircons from the orthogneiss of Angel Lake were supplied by J.E. Wright, Geoscience Department of the University of Georgia, from the same sample (RM-9; Fig. 2) previously analyzed using ID-TIMS methodology.

Zircon Imaging and Morphologies

Transmitted light (TL) images of zircons from sample RM-9 are shown in Figure 3. Based on their morphologies, we subdivided the grains into three main groups: (1) grains that are small to medium size, rounded to subrounded, clear to cloudy (e.g., grains 1, 4, 5, and 9); (2) grains that are similar to group 1 grains except more elongate (e.g., grains 2, 3, and 13); and (3) grains that are clear, euhedral to subhedral, mostly elongate, with dark to almost clear, rounded cores (e.g., grains 5–8, 11, 12, 15, 17, 18, and 20). Data were obtained on both the mostly darker cores and the outer clear rims, and we

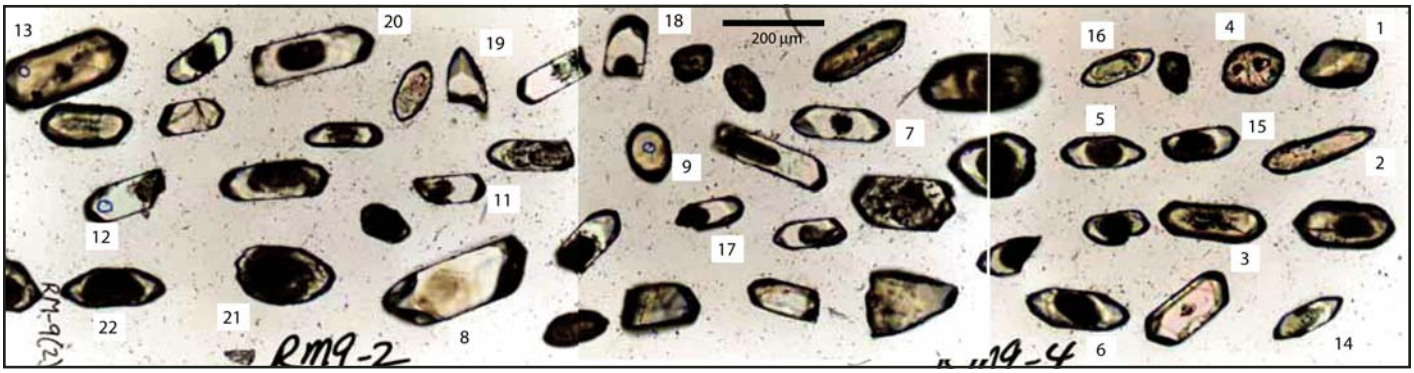

Figure 3. Transmitted light images of zircons separated from sample RM-9, orthogneiss of Angel Lake. Numbers correspond to grain number for sensitive high-resolution ion microprobe spot data in Table 1 and rare earth element data in Table 2. Note rounded dark (metamict) cores within some clear, euhedral to subhedral zircon grains. Other rounded to subrounded to elongate grains vary from clear (transparent) to semi-opaque.

have subdivided these results as groups 3A and 3B, respectively.

CL imaging (Fig. 4) reflects the zoning seen in TL. In general, the zircon grains have lighter, interior regions and darker (higher large ion lithophile element [LILE] content, including uranium) outer regions. The lighter, interior regions of group 1 and 2 grains may or may not exhibit oscillatory zonations; however, most appear to be magmatic in origin. Group 1 grains (rounded to subrounded "seeds") have thin to nonexistent dark rims, suggesting that they were somehow isolated from the magma in which the large overgrowths evident on most of the other grains formed. Group 2 grains have interior regions that are either as light as group 1 grain interior regions or noticeably darker, although not as dark as most exterior regions (Fig. 4), suggesting a difference in LILE contents. Group 2 grains also appear to have interior regions that exhibit some disruption or convoluted zoning (e.g., Hoskin and Black, 2000). Group 3A is characterized by rounded to subrounded cores with variable CL shades from very light (white) to dark (although none is truly black), whereas group 3B exhibits oscillatory zonations indicative of magmatic growth. Group 3B is also typically darker in CL, indicating higher LILE concentrations.

U-Pb Geochronology

SHRIMP spot locations were mainly determined from CL imaging because it elucidates various growth stages. These analyses, therefore, should represent the U-Pb isotopic systematics of zircon formation for specific portions of each grain analyzed. Many of the analyses are concordant and represent closure of the U-Pb system at that age. The SHRIMP-RG U-Th-Pb analytical data are given in Table 1.

The lighter interior regions or cores of group 1 and 2 grains consistently yielded the very latest Archean–earliest Proterozoic $^{207}Pb/^{206}Pb$ ages between 2434 and 2579 Ma (Table 1; red and blue solid ellipses, Figs. 5A, 5B). Of 12 analyses (including all group 1 grains), 9 define a discordia with an upper-intercept age of 2531 ± 19 Ma and a lower-intercept age of 108 ± 91 Ma (mean square of weighted deviates, MSWD = 5.1). These results are comparable to the ID-TIMS results, shown as open circles, that yield an upper-intercept age of 2526 ± 22 Ma (recalculated from Lush et al. [1988] using Ludwig [2003]) and a lower-intercept age of 200 ± 22 Ma (MSWD = 529, assuming correlation coefficient, $\rho = 0.98$). The same 9 SHRIMP analyses yield a mean $^{207}Pb/^{206}Pb$ age of 2516 ± 17 Ma (2516 ± 22 Ma for all 12 analyses).

Three analyses from group 2 grains do not conform to this regression. One of these analyses plots to the right of the discordia, toward an older $^{207}Pb/^{206}Pb$ age of 2579 ± 8 Ma. The other two analyses yield younger $^{207}Pb/^{206}Pb$ ages of 2434 and 2470 Ma (Table 1; Figs. 5A, 5B).

Group 3A analyses yield very discordant results with $^{207}Pb/^{206}Pb$ ages between ca. 1455 and ca. 2170 Ma (Figs. 5C, 5D), and may indicate multiple Pb-loss histories from the original Archean zircon ages. Alternatively, these analyses could represent younger zircon inheritance, because all of the younger $^{207}Pb/^{206}Pb$ ages of ca. 1450, ca. 1600, ca. 1800–1900, ca. 1950, and 2150 Ma are within the ranges of known widespread magmatic episodes in North America.

Fourteen analyses from oscillatory zoned, clear, euhedral, exterior regions (group 3B) yielded $^{206}Pb/^{238}U$ ages between 91 and 72 Ma (Table 1 and Fig. 6). The age data are not concentrated at any one age, but almost evenly distributed along concordia. There is no simple explanation for this isotopic behavior, and we cannot correlate these young ages with any other parameter (e.g., U content or percent common Pb). The weighted mean age for all 14 is 81.0 ± 3.4 Ma (MSWD = 285), although there is little confidence that the real age might be within such a small error. We tentatively suggest that the true age is closer to the oldest analyses, perhaps ca. 90 Ma, and that the other analyses exhibit younger $^{206}Pb/^{238}U$ ages probably as a result of Pb loss. The previously determined mean $^{207}Pb/^{206}Pb$ age of 84.8 ± 2.8 Ma (McGrew et al., 2000) on zircon from a syntectonic leucogranite of the recumbent fold of the Winchell Lake nappe would tend to support such an interpretation.

Trace Element Data

All of the Precambrian zircons, cores or otherwise, exhibited high common Pb (mostly >2.5% of ^{206}Pb), but with variable U contents (~450 to over 3500 ppm; Table 1 and Fig. 7A). In contrast, the clear exterior regions exhibited even higher U contents (3000–4800 ppm), but relatively low common Pb values (<0.5% of ^{206}Pb). These trace element characteristics certainly distinguish these groups as unrelated, a conclusion that is further illustrated by a plot of U versus Th concentrations (Fig. 7B) that show that the groups are reversely correlated, exactly opposite of typical magmatic trends in zircon (e.g., Hoskin and Schaltegger, 2003).

Rare earth element (REE) patterns from data taken concurrently with the U-Th-Pb isotopic data indicate subtle differences between zircons from the different groups (Fig. 8). The two major features are: (1) the uniformity exhibited in the group 3B REE patterns compared to the patterns of the other group, and (2) the relative depletion of the light (L) REEs in the group 3B grains compared to the other

TABLE 1. SHRIMP-RG U-Th-Pb ANALYTICAL DATA FOR ZIRCON COMPONENTS OF THE ORTHOGNEISS OF ANGEL LAKE, EAST HUMBOLDT RANGE, NE NEVADA

Spot name	Spot location	Common ^{206}Pb (%)	U (ppm)	Th (ppm)	$^{232}Th/^{238}U$	Total $^{238}U/^{206}Pb$	Error (%)	Total $^{207}Pb/^{206}Pb$	Error (%)	207-corr. $^{206}Pb/^{238}U$ age	Error (abs)	$^{207}Pb/^{235}U^*$	Error (%)	$^{206}Pb/^{238}U^*$	Error (%)	Error correlation	204-corr. $^{207}Pb/^{206}Pb$ age	Error (abs)	Discordance (%)
RM-9: Orthogneiss of Angel Lake																			
RM9-1	1—mag core	9.35	1255	393	0.32	3.8843	1.6214	0.1663	0.2910	1352	21	5.8978	1.6477	0.2574	1.6214	0.9841	2519	5	46
RM9-1B	1—mag core	7.80	1127	420	0.39	3.3152	0.3578	0.1649	0.3861	1582	6	6.8573	0.5266	0.3016	0.3578	0.6795	2506	6	37
RM9-2	2—mag center	5.18	506	614	1.26	2.6733	1.6479	0.1654	0.3820	1957	32	8.5146	1.6930	0.3740	1.6479	0.9734	2509	7	22
RM9-2B	2—mag center	2.66	458	767	1.73	2.2350	0.5396	0.1722	0.4742	2331	13	10.6222	0.7187	0.4474	0.5396	0.7508	2579	8	9
RM9-3	2—mag center	3.10	916	206	0.23	2.5062	1.7655	0.1580	0.6272	2107	38	8.6886	1.8740	0.3990	1.7655	0.9422	2434	11	13
RM9-3B	2—mag center	2.95	959	215	0.23	2.4265	0.3945	0.1614	0.7257	2169	9	9.1667	0.8270	0.4121	0.3946	0.4771	2470	12	11
RM9-4	1—core	8.44	753	318	0.44	3.6030	1.6338	0.1639	0.4907	1460	23	6.2746	1.7060	0.2776	1.6339	0.9577	2497	8	42
RM9-4B	1—core	9.45	483	225	0.48	4.2787	0.6010	0.1616	0.6972	1238	8	5.2045	0.9228	0.2337	0.6012	0.6515	2472	12	50
RM9-5.1	3A—dark core	7.10	1041	232	0.23	5.3424	1.6396	0.1332	0.6961	1034	16	3.4327	1.7825	0.1871	1.6396	0.9198	2138	12	52
RM9-5.1B	3A—dark core	7.18	1178	351	0.31	5.1005	0.3918	0.1356	0.5467	1078	4	3.6648	0.6741	0.1960	0.3918	0.5813	2171	10	51
RM9-5.2	3B—clear rim	-0.05	3526	30	0.01	88.5575	0.4040	0.0471	1.5632	72.4	0.3								
RM9-6.1	3A—dark core	7.14	2327	112	0.05	11.0959	1.6215	0.1158	0.3766	518	8.2	1.4294	1.6728	0.0900	1.6216	0.9694	1882	7	74
RM9-6.1B	3A—dark core	8.02	2213	96	0.04	11.1927	0.3021	0.1226	0.5689	509	1.8	1.5025	0.7322	0.0893	0.3072	0.4195	1987	12	75
RM9-6.2	3B—clear rim	-0.11	3287	36	0.01	81.5084	0.3687	0.0467	1.4105	78.7	0.3								
RM9-7	3B—clear rim	0.02	3593	32	0.01	76.3215	1.6482	0.0479	1.2466	83.9	1.4								
RM9-8.1	3B—clear rim	0.11	4079	39	0.01	78.3231	1.6437	0.0485	1.1795	81.7	1.3								
RM9-8B	3B—clear rim	0.11	4511	24	0.01	70.6411	0.4344	0.0487	1.6149	90.5	0.4								
RM9-8.2	1—core	9.70	1234	137	0.11	4.5154	1.6316	0.1610	0.7110	1175	19	4.9056	1.7813	0.2214	1.6316	0.9160	2463	12	9
RM9-8.2B	1—core	0.36	776	168	0.22	2.1275	0.4493	0.1652	0.9932	2476	13	10.6943	1.0925	0.4700	0.4495	0.4115	2508	17	53
RM9-9	1—core	2.65	814	320	0.41	2.2814	1.6301	0.1687	0.3182	2291	39	10.1850	1.6614	0.4382	1.6301	0.9811	2543	5	2
RM9-11	3B—clear rim	0.23	4097	45	0.01	89.1807	1.6481	0.0493	1.2436	71.7	1.2								
RM9-12	3B—clear rim	0.02	4749	36	0.01	72.8497	1.6360	0.0479	1.0684	87.9	1.4								
RM9-13	2—mag center	2.71	1235	229	0.19	2.2984	1.6271	0.1679	0.5129	2276	38	10.0775	1.7060	0.4351	1.6271	0.9537	2538	9	10
RM9-14	2—convoluted	6.28	2662	33	0.01	31.7389	0.3256	0.0999	1.3146	188	0.7	0.4332	1.3622	0.0315	0.3260	0.2393	1619	25	89
RM9-15.1	3B—clear rim	-0.03	3597	40	0.01	78.1930	0.3885	0.0474	1.2804	81.9	0.3								
RM9-15.2	3A—dark core	6.51	1883	77	0.04	9.5290	0.2318	0.1132	0.9445	603	1.8	1.6343	0.9776	0.1049	0.2321	0.2374	1848	17	69
RM9-16	2—mag rim	6.20	3592	116	0.03	37.4495	0.2852	0.0986	0.7229	159	0.5	0.3598	0.8450	0.0267	0.2880	0.3409	1583	15	91
RM9-17	3B—clear rim	0.01	3925	22	0.01	72.6046	0.3186	0.0478	1.2062	88.2	0.3								
RM9-18	3B—clear rim	-0.04	4287	46	0.01	74.9141	0.3102	0.0474	1.1737	85.5	0.3								
RM9-19	3B—clear rim	-0.15	4121	37	0.01	75.1545	0.3211	0.0465	1.2296	85.3	0.3								
RM9-20	3B—clear rim	0.06	3556	36	0.01	87.7167	0.3788	0.0480	1.4423	73.0	0.3								
RM9-21.1	3B—clear rim	-0.13	3175	41	0.01	78.8733	0.3703	0.0466	1.4113	81.3	0.3								
RM9-21.2	3A—dark core	7.48	2387	120	0.05	9.5991	0.1953	0.1208	0.4395	593	1.5	1.7254	0.4994	0.1041	0.1963	0.3931	1959	8	71
RM9-22.1	3B—clear rim	0.53	3372	37	0.01	82.9978	0.3603	0.0517	1.6037	76.8	0.3								
RM9-22.2	3A—dark core	4.55	2182	106	0.05	11.4027	0.2109	0.0947	0.4480	518	1.2	1.1017	0.6767	0.0873	0.2173	0.3211	1457	12	66

Note: Group numbers and short core/rim designations are given in second column; see text for explanation of group numbers. “mag” refers to a zone with oscillatory zoning indicative of magmatic zircon growth. All errors are given at the 1σ. SHRIMP-RG—sensitive high-resolution ion microprobe–reverse geometry; corr—corrected.

*Radiogenic.

TABLE 2. CHONDRITE-NORMALIZED RARE EARTH ELEMENT DATA FROM ZIRCONS FROM THE ORTHOGNEISS OF ANGEL LAKE, EAST HUMBOLDT RANGE, NORTHEASTERN NEVADA

Spot name	La	Ce	Pr	Nd	Sm	Eu	Gd	Dy	Er	Yb	Ce/Ce*	Eu/Eu*
Group 1												
RM-9-B1	2.16	7.83	5.02	7.65	45.43	0.58	270.9	749	1871	2816	2.38	0.01
RM-9-B4	2.18	19.44	1.96	1.85	9.37	4.75	59.0	187	533	966	9.42	0.20
RM-9-B10	0.24	4.20	0.66	1.09	11.59	0.30	93.8	355	1083	1809	10.57	0.01
Group 2												
RM-9-B2	4.29	47.50	11.83	19.64	65.93	38.02	263.4	444	854	1138	6.66	0.29
RM-9-B3	0.99	5.78	1.24	1.38	14.32	0.48	115.1	420	1222	2015	5.21	0.01
RM-9-14	10.35	3.70	2.93	1.56	3.88	1.69	28.4	216	857	2103	0.67	0.16
RM-9-16.1	2.40	7.60	1.10	0.75	4.59	3.42	48.7	225	551	686	4.67	0.23
Group 3A												
RM-9-B5	8.59	18.89	5.12	3.95	22.03	1.22	135.2	445	1241	2086	2.85	0.02
RM-9-B6	5.73	5.86	2.40	1.56	8.08	0.41	81.1	253	409	482	1.58	0.02
RM-9-15.2	22.34	10.08	4.92	2.31	6.09	2.36	47.9	277	956	1754	0.96	0.14
RM-9-21.2	4.92	5.45	2.32	1.59	9.71	1.12	79.7	317	684	861	1.61	0.04
RM-9-22.2	5.73	6.96	2.75	1.91	11.36	4.79	84.7	260	447	536	1.75	0.15
Group 3B												
RM-9-5.2	0.55	1.20	0.23	0.15	2.20	0.45	29.3	239	807	1571	3.38	0.06
RM-9-6.2	0.35	1.37	0.20	0.15	2.42	0.31	31.1	234	599	717	5.25	0.04
RM-9-B8	0.08	1.23	0.15	0.20	1.96	0.90	29.9	255	1562	6166	11.57	0.12
RM-9-15.1	0.40	1.27	0.32	0.28	2.24	0.22	32.8	282	973	1271	3.56	0.03
RM-9-17.1	4.05	1.61	0.50	0.18	2.48	0.50	30.1	249	839	1300	1.12	0.06
RM-9-18.1	0.15	1.80	0.17	0.19	2.82	0.39	41.8	324	1008	1354	11.36	0.04
RM-9-19.1	0.18	1.60	0.16	0.16	2.52	0.42	35.9	300	939	1286	9.26	0.04
RM-9-20.1	0.22	1.25	0.15	0.12	2.39	0.25	29.5	242	835	1591	7.02	0.03
RM-9-21.1	0.23	1.11	0.17	0.15	2.26	0.29	30.2	219	621	766	5.62	0.03
RM-9-22.1	2.93	1.88	0.99	0.57	2.88	1.18	27.2	232	1265	3030	1.10	0.13
% error ± 1σ	15	4	4	4	4	4	4	3	2	2	10	4

groups. For example, the cerium content of the group 3B grains is on average one order of magnitude less than that seen in the other groups. This fact is further illustrated on a Ce/Sm versus Dy/Sm diagram that compares the steepness of the LREE pattern to that between the LREEs and the heavy (H) REEs (Fig. 9), and shows not only the uniformity of the LREE behavior of the Cretaceous group 3B grains (Ce/Sm = 2.0–2.7 and Dy/Sm > 130), but also the contrasting variability of the Precambrian zircon components (Ce/Sm = 0.7–8.5 and Dy/Sm <95). Once again, these trace element characteristics indicate that these groups are not derived from the same igneous source.

The trace element characteristics of zircon are not likely to be altered during metamorphism unless their U-Pb ages are also reset. Therefore, the compositional differences between the Cretaceous and Precambrian age zones reflect the composition of zircon grown at the U-Pb ages of the zircon domains. The oscillatory zoning typical of magmatic growth is usually lost when zircons are recrystallized or dissolved, and regrown during metamorphic events.

DISCUSSION

The SHRIMP-RG data confirm the existence of Archean zircon grains or Archean components within zircon grains of this sample, but the combined evidence strongly suggests that this orthogneissic unit is a highly deformed, Late Cretaceous monzogranite derived from melting of a source containing detritus with an abundance of Archean zircons. These new data negate the existence of Archean crust within the Winchell Lake nappe.

Evidence that the Precambrian Grains Are Detrital

(1) We interpret the morphologies of group 1 grains and group 3 cores to be detrital in nature (Figs. 3 and 4); particularly grain 9, which is well rounded with the original magmatic oscillatory zonations truncated by abrasive action during sediment transport. This grain also does not contain an overgrowth, and several other Archean grains have only thin overgrowths (e.g., grain 2 and possibly 13; Figs. 3 and 4). These observations indicate that some of the Archean grains were protected from the Cretaceous melt, likely in xenocrystic clots of the country rock that was not entirely digested by the Cretaceous melt. (2) There is a wide range of $^{207}Pb/^{206}Pb$ ages (~140 m.y.) in the earliest Proterozoic–latest Archean grains (Fig. 5B) that is certainly suggestive of multiple sources, and is significantly greater than typical external errors of SHRIMP $^{207}Pb/^{206}Pb$ data for zircon from Early Proterozoic and Archean igneous rocks (e.g., <4% at 2500 Ma; i.e., the age variation is real, and not analytical).

(3) Although highly discordant, Proterozoic ages were also obtained from the rounded to subrounded cores of zircon grains with Late Cretaceous outer zones (Fig. 4). These analyses yielded ages that coincide with known regional magmatic events in North America: ca. 1615 Ma (late Mazatzal); 1850 and 1880 Ma (Trans-Hudsonian); 1960 and 1990 Ma (Penokean); 2140 and 2170 Ma (Selway, or similar to ages for mafic dike intrusions throughout the Wyoming and Superior Provinces); and one at 1460 Ma (Fig. 5D). Some of these Proterozoic ages are similar to those found in zircons analyzed from Late Cretaceous–Oligocene plutons to the south in Lamoille Canyon (Fig. 1; Premo, 2008, personal observ.). They exhibit a similar Mesoproterozoic–Paleoproterozoic and Late Archean detrital zircon inheritance, evidence that supports the contention that the sedimentary sequences (Neoproterozoic–Paleozoic) between the East Humboldt Range and the Ruby Mountains are related, although the East Humboldt Range sequences appear to be dominated by Archean detritus, and the Ruby Mountains appear to be dominated by detritus from Proterozoic sources.

(4) The variations in the REE patterns and other trace element data from zircon components of groups 1–3A (Figs. 7–9) indicate that most of these zircons are not from the same igneous source, further evidence that they are detrital in origin. Likewise, the uniformity of the REE patterns and other trace element correlations in the Late Cretaceous rims indicates that they are related and most likely from the same or similar igneous source.

Age and Source of the Detritus

Judging from this sample's Nd isotopic signature of −34.6 (at 35 Ma; Wright and Snoke,

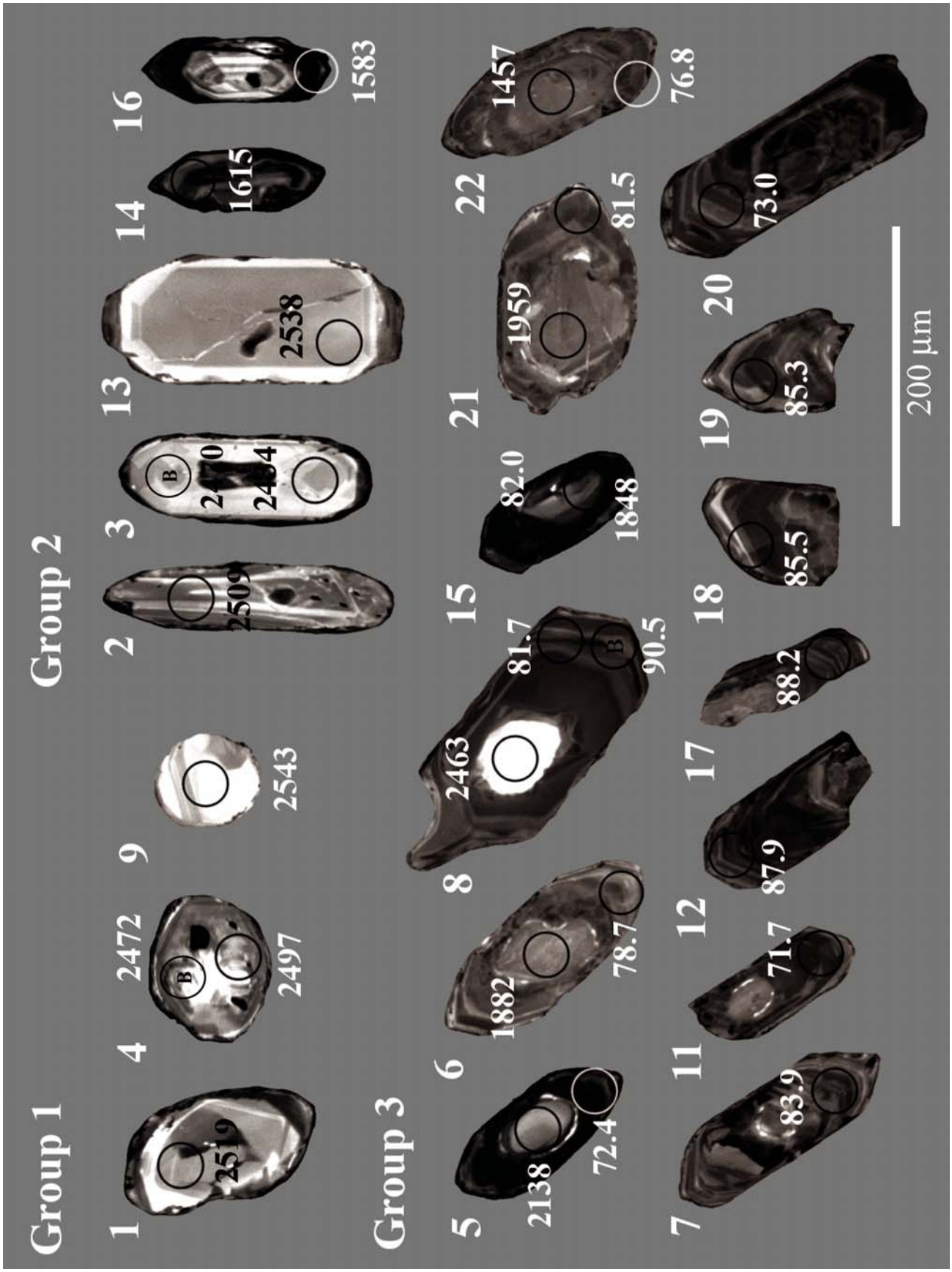

Figure 4. Cathodoluminescence images of zircons separated from sample RM-9, orthogneiss of Angel Lake. Ovoids indicate locations of spot craters (analyzed areas). Note that inner, nonzoned areas are both U poor (light-colored) and U rich (dark), and yield Proterozoic–Late Archean ages, whereas outer oscillatory zoned areas yield Late Cretaceous ages.

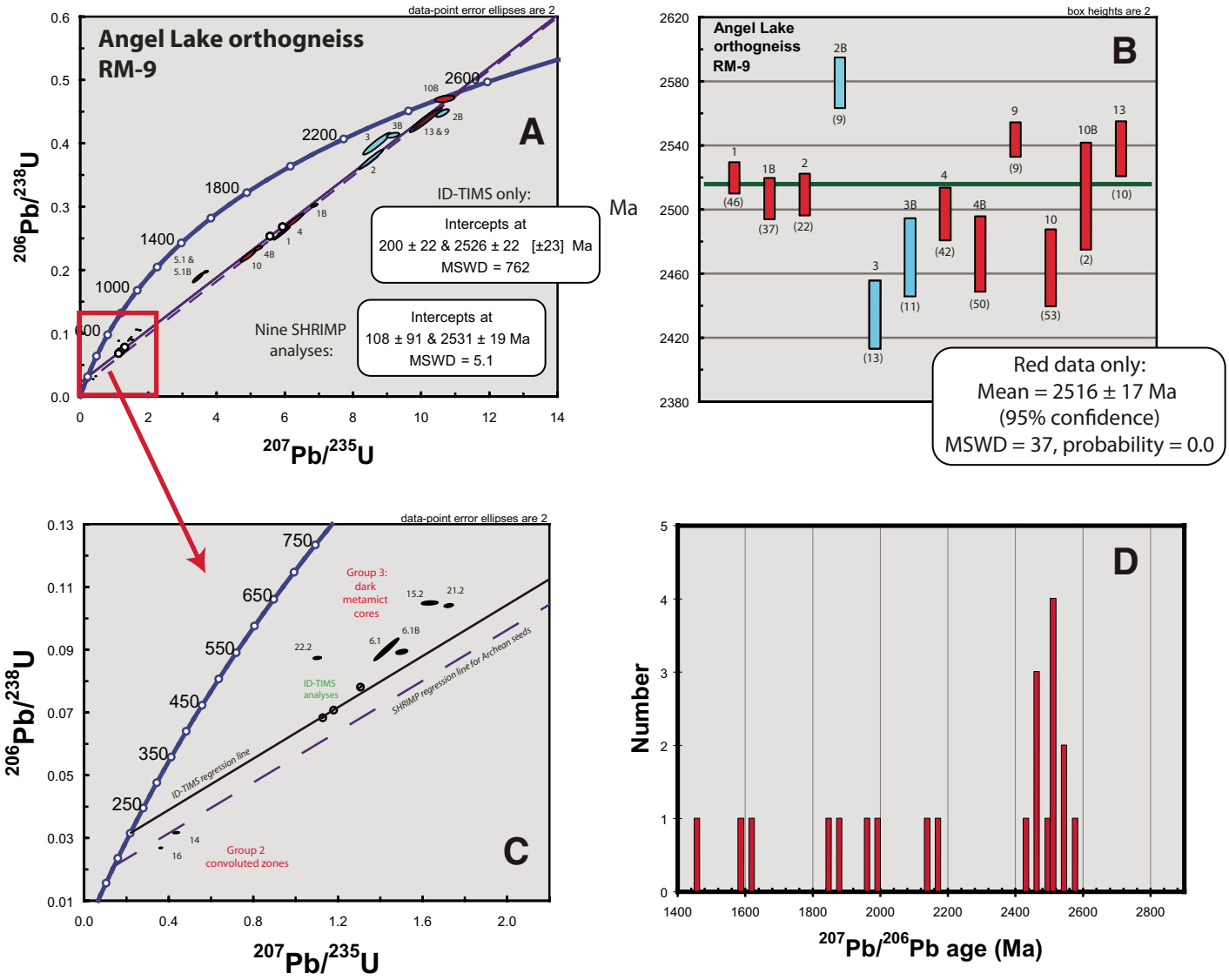

Figure 5. (A) Conventional concordia diagram comparing sensitive high-resolution ion microprobe (SHRIMP) data (solid ellipses) from this study and isotope dilution–thermal ionization mass spectrometry (ID-TIMS) data (open circles) from Lush et al. (1988). Red ellipses are included in the SHRIMP regression; blue ellipses are not. See text for further explanation. MSWD—mean square of weighted deviates. (B) Age comparison diagram for the Late Archean–earliest Proterozoic zircon age results, illustrating the scatter in $^{207}Pb/^{206}Pb$ ages obtained from both zircon grains and cores. Numbers over the age error bars correspond to the spot number given in Table 1. Numbers in parentheses under each age error bar indicate percent discordance of that analysis. Red bars are included in the SHRIMP regression; blue bars are not. (C) Inset of diagram A showing U-Pb results of the most discordant analyses. Note all of these analyses plot off both the ID-TIMS and the SHRIMP regression chords for Archean zircon components. (D) Diagram illustrating the distribution of $^{207}Pb/^{206}Pb$ ages from suspected detrital zircon components. Note that suspected inherited Proterozoic ages occur at known regional magmatic ages.

1993), the sedimentary source could have been composed entirely of Archean crust with an average age of ca. 3.05 Ga, even though no zircons older than 2.6 Ga were found in this sample. The average 2.54 Ga age for the Archean zircon components in this sample suggests a source very similar to rocks in the Grouse Creek–Albion–Raft River metamorphic core complex of northwestern Utah, ~250 km northeast of the Ruby Mountains–East Humboldt Range. Some recently reported SHRIMP U-Pb zircon ages from plutonic rocks are similar to the age data from the monzogranitic orthogneiss of Angel Lake, yielding lower-intercept ages between 80 and 100 Ma, and upper-intercept ages of ca. 2550 Ma (Strickland et al., 2007). However, Strickland et al. (2007) interpret the younger age as representing secondary zircon growth during the Late Cretaceous and the older age as the basement protolith age.

The depositional age of the sediment currently remains elusive and could be earliest Proterozoic to Cretaceous, although it is likely to be Late Proterozoic to earliest Paleozoic, as are many of the oldest exposed siliciclastic detrital packages in this region of the Great Basin. If one can believe the youngest provenance age indicated by inherited zircon from this sample, an upper limit of ca. 1450 Ma might be applied to the age of deposition for the sediment.

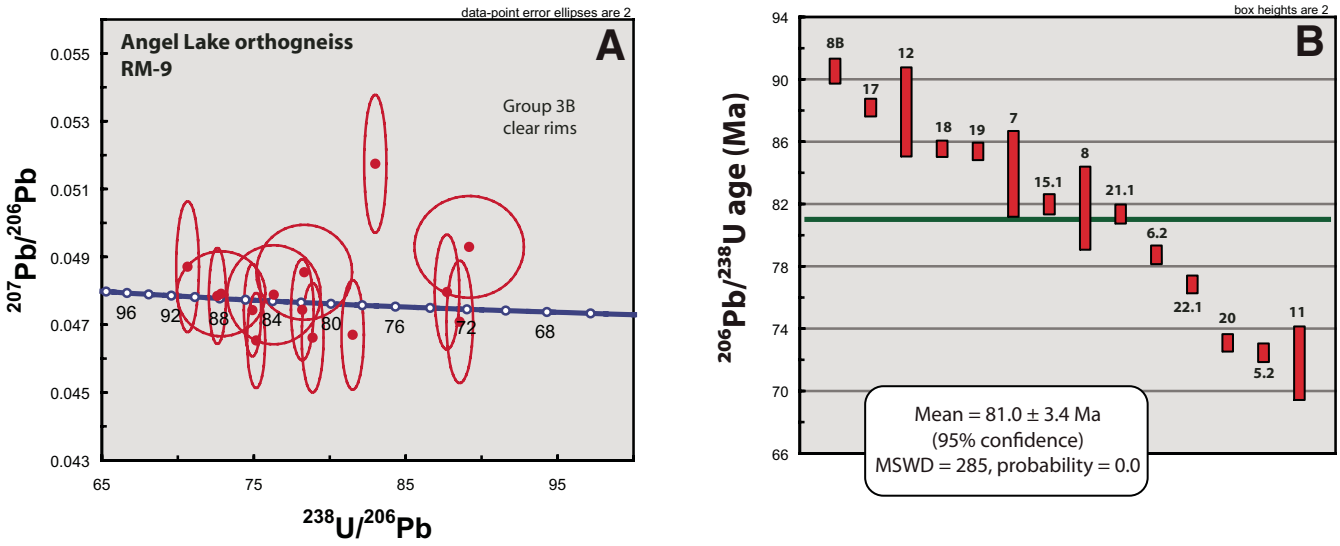

Figure 6. (A) Tera-Wasserburg plot of analyses from oscillatory zoned magmatic rims (Figs. 3 and 4) indicating a range of near-concordant $^{206}Pb/^{238}U$ ages between 91 and 72 Ma. High U concentrations (>3000 ppm) are likely to have disturbed the U-Pb systematics of some grains, resulting in inconsistent U-Pb age results. Whereas the true protolithic age of this orthogneiss is uncertain, we prefer an age of ca. 90 Ma, and the other analyses may exhibit younger ages due to Pb loss. (B) A weighted mean age can be calculated at 81 ± 3.4 Ma, but we have little confidence that the true age is within these errors. Spot numbers are indicated over each age error bar.

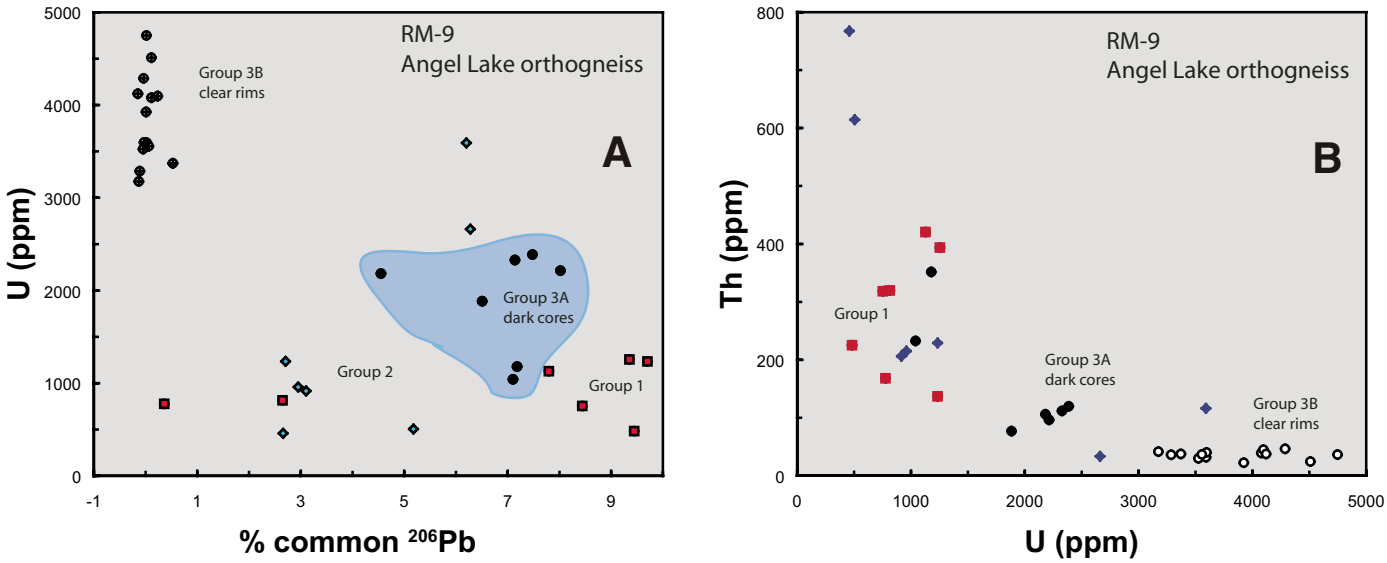

Figure 7. (A) U (ppm) versus percent common ^{206}Pb for all zircon components analyzed. Note the scatter in groups 1 and 2 (red squares and blue diamonds, respectively), and the relative uniformity of groups 3A and 3B (black circles and circles with crosses, respectively). Also, clear magmatic rims on grains from group 3B are much higher in U contents (>3000 ppm) compared to the other groups. (B) Th (ppm) versus U (ppm) for all the zircon grains analyzed. Note the scatter in groups 1 and 2, and the relative uniformity of groups 3A and 3B, which are low in Th relative to U (Th/U <0.1), indicating a melt very likely derived from a metamorphic fluid.

Implications for the Timing of Late Cretaceous Magmatism

The SHRIMP-RG age data for the orthogneiss of Angel Lake (Fig. 6) is interpreted with confidence as Late Cretaceous, but cannot be more precisely defined with this data. The very high U concentrations (>3000 ppm) of the Late Cretaceous magmatic rims undoubtedly have caused some crystal lattice deformation and indicate the likelihood of small percentages of Pb redistribution, which may result in the poor U-Pb isotopic behavior exhibited in these analyses. Nonetheless, we speculate that the protolith igneous age of this orthogneiss is ca. 90 Ma and that the slightly younger $^{206}Pb/^{238}U$ ages are the result of Pb loss. This interpretation is supported by the occurrence of another orthogneiss at

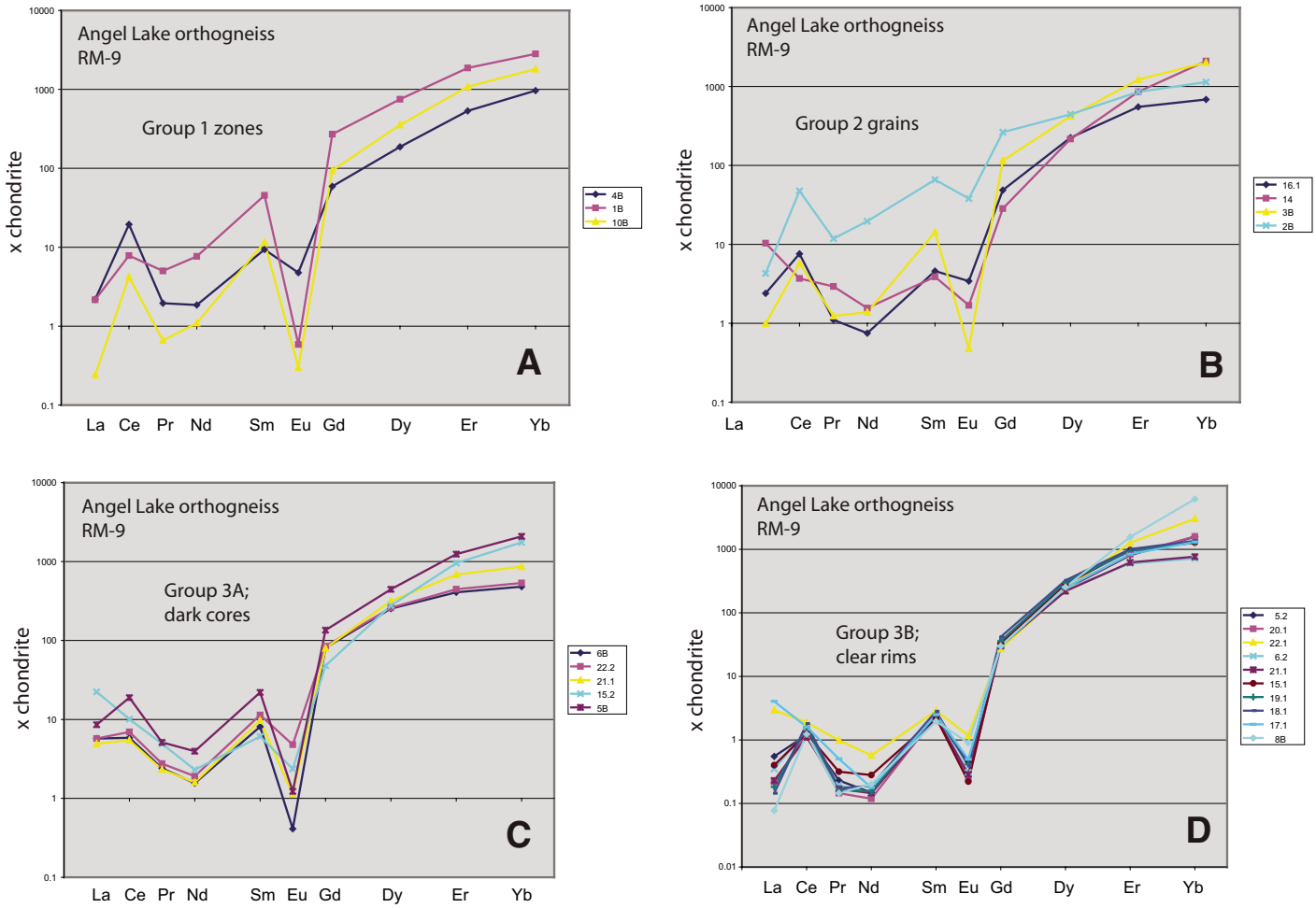

Figure 8. (A) Rare earth element (REE) patterns for the group 1 Archean zircon grains, illustrating some significant differences (Eu anomaly and relative abundances), evidence for source differences, and a detrital origin. (B) REE patterns for the group 2 Archean and Proterozoic zircon grains, illustrating some significant differences (Eu anomaly and relative abundances), evidence for source differences, and a detrital origin. (C) REE patterns for the group 3A dark cores, and, although better behaved than patterns shown in A or B, some abundance differences remain. (D) REE patterns for the group 3B Cretaceous magmatic rims, illustrating the relatively uniform contents at 8 out of 10 spots. Two analyses (8B and 22.1) stray slightly. Note also that the light REEs are depleted on average ~10× those of the older zircon components.

Thorpe Creek in Lamoille Canyon to the south (Fig. 1) that yielded a dominant $^{206}Pb/^{238}U$ age of 92 ± 1 Ma and the mean $^{207}Pb/^{206}Pb$ age of 84.8 ± 2.8 Ma (McGrew et al., 2000) on zircon from a syntectonic leucogranite of the recumbent fold of the Winchell Lake nappe.

These ages are similar to recently reported SHRIMP U-Pb zircon ages from plutonic rocks of the Grouse Creek–Albion–Raft River metamorphic core complex of northwestern Utah that yield lower-intercept ages between 80 and 100 Ma (Strickland et al., 2007). The combined results support the occurrence of a plutonic event ca. 90–95 Ma in this region (Du Bray, 2007), an event that is well documented in Late Cretaceous magmatic arcs farther west.

Age of Orthogneiss Formation

Other U-Pb ages in the Angel Lake area are notably younger and include a U-Pb zircon age of 40 ± 3 Ma for a quartz dioritic orthogneiss just south of Angel Lake as well as a U-Pb monazite age of 29 ± 0.5 Ma from a biotite monzogranitic orthogneiss at Angel Lake (Wright and Snoke, 1993). Most dated samples of Late Cretaceous–mid-Tertiary monzogranitic to leucogranitic magmatic rocks (between ca. 90 and 29 Ma; Wright and Snoke, 1993) contain some degree of mylonitic or related deformational fabric such that mylonitization associated with core complex formation either was concurrent with or postdated the youngest magmatic events at ca. 29 Ma. These ages are also comparable to ages for samples from rocks of similar composition from the Grouse Creek–Albion–Raft River metamorphic core complex (Egger et al., 2003; Strickland et al., 2007).

Implications for the Distribution of Archean and Proterozoic Basement

Previous studies in northeast Nevada have delineated Precambrian crustal basement based on significant changes in the Pb, Sr, Nd, or O isotopic compositions of whole rocks or minerals from Mesozoic and Tertiary plutonic rocks (Kistler and Peterman, 1973, 1978; Farmer and DePaolo, 1983, 1984; DePaolo and Farmer,

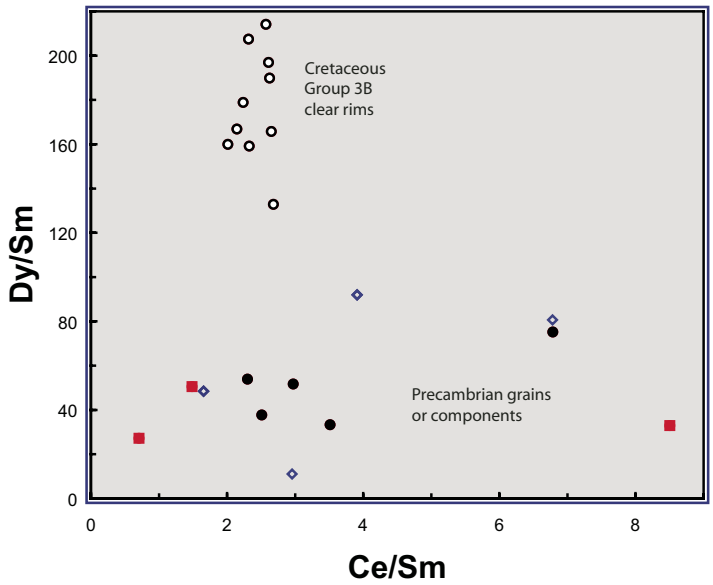

Figure 9. Dy/Sm versus Ce/Sm for all zircon components analyzed. This plot further illustrates the depletion of light rare earth element (LREEs) within group 3B Cretaceous magmatic rims and the scatter or spread in LREE abundances in the different Precambrian zircon components.

1984; Bennett and DePaolo, 1987; Wright and Wooden, 1991; Wright and Snoke, 1993; Farmer and Ball, 1997; Wooden et al., 1998; Tosdal et al., 1998, 2003; Vikre, 2000; King et al., 2004) or by geophysical methodology (Allmendinger et al., 1987; Grauch et al., 2003; Rodriguez and Williams, 2008, 2008). Wright and Snoke (1993) proposed that the Archean-Proterozoic boundary crossed the East Humboldt Range based on distinct differences in Nd signatures from samples within the East Humboldt Range as opposed to samples from the Ruby Mountains to the south; the former exhibits initial ε_{Nd} values of <–20, indicating the probability of a major Archean crustal component in their production. However, it is possible that sediments, largely derived from Archean crust, can exhibit these same isotopic signatures and influence the isotopic signatures of plutonic rocks derived from or assimilating significant amounts of sediment with Archean signatures.

While previous researchers have identified the orthogneiss of Angel Lake (and particularly the sample, RM-9) as the best candidate for an Archean rock in the East Humboldt Range, our new age data indicate that there are no Archean crustal rocks exposed in the East Humboldt Range. If this is so, then the Archean-Proterozoic boundary does not exist in the Ruby Mountains–East Humboldt Range. This contention is supported by new two-dimensional resistivity modeling of magnetotelluric sounding profiles that suggest that the Archean-Proterozoic boundary is ~50 km to the northeast of the Ruby Mountains–East Humboldt Range and trends to the northwest across the Goshute-Toano Ranges and the Pequop Mountains (Rodriguez and Williams, 2008).

If the geophysical interpretation is correct, then the gneisses at Angel Lake in the East Humboldt Range are probably underlain by the Mojave Province and Neoproterozoic and/or Paleozoic siliciclastic sedimentary sequences derived primarily from either the Wyoming Province or the Grouse Creek–Albion–Raft River complex, or both. Farther south, in the Ruby Mountains (Lamoille Canyon), a greater proportion of the detrital zircon present in Late Cretaceous–Oligocene plutons was derived from Proterozoic rocks (Premo, 2008, personal observ.).

Implications for the Origin of Carlin-Type Gold Deposits

Howard (2003) suggested that rocks similar to the deep crustal rocks exposed in the Ruby Mountains–East Humboldt Range may have underlain the Carlin Trend during the mid-Tertiary, and therefore may represent the source rocks for the gold deposits. With the apparent absence of Archean crust in the Ruby Mountains–East Humboldt Range, it becomes more probable that some of the gold in mid-Tertiary hydrothermal deposits of the world-class Carlin and Battle Mountain–Eureka trends and neighboring mining districts in Nevada was leached from Neoproterozoic and Paleozoic siliciclastic sediments derived from crystalline rocks of the Archean and Proterozoic craton.

SUMMARY

(1) The protolith of the orthogneiss of Angel Lake was a Late Cretaceous (ca. 90 Ma) monzogranitic igneous body that was derived from melting of an older sedimentary sequence dominated by Archean detritus. These rocks were later folded and metamorphosed during Late Cretaceous–mid-Tertiary tectonic activity probably related to core complex formation. While these new SHRIMP age data negate the existence of Archean crust in the Winchell Lake nappe, they do not preclude the possibility that Archean crust exists at depth within this region. However, the geophysical data suggest that this region is underlain by crystalline rocks of the Mojave Province.

(2) If it is correct that rocks now exposed in the Ruby Mountains–East Humboldt Range may have underlain the Carlin gold trend, as suggested by Howard (2003), then our new age data would suggest that the gold source is not intact Archean crust, but probably Neoproterozoic and/or Paleozoic sediments derived primarily from Archean crust in some strata and Proterozoic crust in others.

ACKNOWLEDGMENTS

This work was supported by the U.S. Geological Survey's Mineral Resources Program under the Metallogeny of the Great Basin project. We would like to thank James E. "Jim" Wright at the University of Georgia for contributing a portion of his zircons from sample RM-9, the orthogneiss of Angel Lake, and Paul Mueller and Keith Howard for their thorough reviews. We are also thankful to Isabelle Brownfield and Heather Lowers at the Microbeam Lab under the supervision of Greg Meeker at the USGS in Denver for their assistance in CL imaging of the zircon grains. Last, but not least, our thanks to the efficient and attentive workers of the SUMAC laboratories at Stanford University (Frank Mazdab, Bettina Wiegand, Brad Ito, and Ariel Strickland, among others) for their help in operating the SHRIMP instrumentation and in interpreting the results—all are greatly appreciated.

REFERENCES CITED

Allmendinger, R.W., Hauge, T.A., Hauser, E.C., Potter, C.J., Klemperer, S.L., Nelson, K.D., Knuepfer, P., and Oliver, J., 1987, Overview of the COCORP 40°N Transect, western United States: The fabric of an orogenic belt: Geological Society of America Bulletin, v. 98, p. 308–319, doi: 10.1130/0016-7606(1987)98<308:OOTCNT>2.0.CO;2.

Bennett, V.C., and DePaolo, D.J., 1987, Proterozoic crustal history of the western United Sates as determined by neodymium isotopic mapping: Geological Society of America Bulletin, v. 99, p. 674–685, doi: 10.1130/0016-7606(1987)99<674:PCHOTW>2.0.CO;2.

Black, L.P., Kamo, S.L., Allen, C.M., Davis, D.W., Aleinikoff, J.N., Valley, J.W., Mundil, R., Campbell,

I.H., Korsch, R.J., Williams, I.S., and Foudoulis, C., 2004, Improved $^{206}Pb/^{238}U$ microprobe geochronology by the monitoring of a trace-element-related matrix effect, SHRIMP, ID-TIMS, ELA-ICP-MS and oxygen isotope documentation for a series of zircon standards: Chemical Geology, v. 205, p. 115–140, doi: 10.1016/j.chemgeo.2004.01.003.

Cameron, E.M., 1988, Archean gold: Relation to granulite formation and redox zoning in the crust: Geology, v. 16, p. 109–112, doi: 10.1130/0091-7613(1988)016<0109:AGRTGF>2.3.CO;2.

Crittenden, M.D., Jr., Coney, P.J., and Davis, G.H., eds., 1980, Cordilleran metamorphic core complexes: Geological Society of America Memoir 153, 490 p.

Davis, D.W., Williams, I.S., and Krogh, T.E., 2003, Historical development of zircon geochronology, *in* Hanchar, J.M., and Hoskin P.W.O., eds., Zircon: Mineralogical Society of America Reviews in Mineralogy and Geochemistry, v. 53, p. 145–181.

DePaolo, D.J., and Farmer, G.L., 1984, Isotopic data bearing on the origin of Mesozoic and Tertiary granitic rocks in the western United States: Royal Society of London Philosophical Transactions, ser. A, v. 310, p. 743–753, doi: 10.1098/rsta.1984.0017.

Du Bray, E.A., 2007, Time, space, and composition relations among northern Nevada intrusive rocks and their metallogenic implications: Geosphere, v. 3, no. 5, p. 381–405, doi: 10.1130/GES00109.1.

Egger, A.E., Dumitru, T.A., Miller, E.L., Savage, C.F.I., and Wooden, J.L., 2003, Timing and nature of Tertiary plutonism and extension in the Grouse Creek Mountains, Utah: International Geology Review, v. 45, p. 497–532, doi: 10.2747/0020-6814.45.6.497.

Farmer, G.L., and Ball, T.T., 1997, Sources of Middle Proterozoic to Early Cambrian siliciclastic sedimentary rocks in the Great Basin: A Nd isotope study: Geological Society of America Bulletin, v. 109, p. 1193–1205, doi: 10.1130/0016-7606(1997)109<1193:SOMPTE>2.3.CO;2.

Farmer, G.L., and DePaolo, D.J., 1983, Origin of Mesozoic and Tertiary granites in the western U.S. and implications for pre-Mesozoic crustal structure, 1. Nd and Sr isotopic studies in the geocline of the northern Great Basin: Journal of Geophysical Research, v. 88, p. 3379–3401, doi: 10.1029/JB088iB04p03379.

Farmer, G.L., and DePaolo, D.J., 1984, Origin of Mesozoic and Tertiary granites in the western U.S. and implications for pre-Mesozoic crustal structure, 2. Nd and Sr isotopic studies of unmineralized and Cu- and Mo-mineralized granites in the Precambrian craton: Journal of Geophysical Research, v. 89, p. 10,141–10,160, doi: 10.1029/JB089iB12p10141.

Grauch, V.J.S., Rodriguez, B.D., and Wooden, J.L., 2003, Geophysical and isotopic constraints on crustal structure related to mineral trends in north-central Nevada and implications for tectonic history: Economic Geology, v. 98, p. 269–286.

Hoskin, P.W.O., and Black, L.P., 2000, Metamorphic zircon formation by solid-state recrystallization of protolith igneous zircon: Journal of Metamorphic Geology, v. 18, p. 423–439, doi: 10.1046/j.1525-1314.2000.00266.x.

Hoskin, P.W.O., and Schaltegger, U., 2003, The composition of zircon and igneous and metamorphic petrogenesis, *in* Hanchar, J.M., and Hoskin, P.W.O., eds., Zircon: Mineralogical Society of America Reviews in Mineralogy and Geochemistry, v. 53, p. 27–62.

Howard, K.A., 1966, Structure of the metamorphic rocks of the northern Ruby Mountains, Nevada [Ph.D. thesis]: New Haven, Connecticut, Yale University, 170 p.

Howard, K.A., 1980, Metamorphic infrastructure in the northern Ruby Mountains, Nevada, *in* Crittenden, M.D., Jr., Coney, P.J., and Davis, G.H., eds., Cordilleran metamorphic core complexes: Geological Society of America Memoir 153, p. 335–347.

Howard, K.A., 2000, Geology of the Lamoille Quadrangle, Elko County, Nevada: Nevada Bureau of Mines and Geology Map 125, scale 1:24,000.

Howard, K.A., 2003, Crustal structure in the Elko-Carlin region, Nevada, during Eocene gold mineralization: Ruby-East Humboldt metamorphic core complex as a guide to the deep crust: Economic Geology and the Bulletin of the Society of Economic Geologists, v. 98, p. 249–268.

Howard, K.A., Kistler, R.W., Snoke, A.W., and Willden, R., 1979, Geologic map of the Ruby Mountains, Nevada: U.S. Geological Survey Miscellaneous Investigations Series Map I-1136, scale 1:125,000.

Ireland, T.R., and Williams, I.S., 2003, Considerations in zircon geochronology by SIMS, *in* Hanchar, J.M., and Hoskin, P.W.O., eds., Zircon: Mineralogical Society of America Reviews in Mineralogy and Geochemistry, v. 53, p. 215–241.

King, E.M., Valley, J.W., Stockli, D.F., and Wright, J.E., 2004, Oxygen isotope trends of granitic magmatism in the Great Basin: Location of the Precambrian craton boundary as reflected in zircons: Geological Society of America Bulletin, v. 116, p. 451–462, doi: 10.1130/B25324.1.

Kistler, R.W., and Peterman, Z.E., 1973, Variations in Sr, Rb, K, Na, and initial $^{87}Sr/^{86}Sr$ in Mesozoic granitic rocks and intruded wall rocks in central California: Geological Society of America Bulletin, v. 84, p. 3489–3512, doi: 10.1130/0016-7606(1973)84<3489:VISRKN>2.0.CO;2.

Kistler, R.W., and Peterman, Z.E., 1978, Reconstruction of crustal blocks of California on the basis of initial strontium isotopic compositions of Mesozoic granitic rocks: U.S. Geological Survey Professional Paper 1071, 17 p.

Ludwig, K.R., 2002, SQUID 1.02, a user's manual: Berkeley Geochronology Center Special Publication 2, 17 p.

Ludwig, K.R., 2003, ISOPLOT/Ex, version 3, A geochronological toolkit for Microsoft Excel: Berkeley Geochronology Center Special Publication 4, 71 p.

Lush, A.P., 1982, Geology of part of the northern East Humboldt Range, Elko County, Nevada [M.S. thesis]: Columbia, University of South Carolina, 138 p.

Lush, A.P., McGrew, A.J., Snoke, A.W., and Wright, J.E., 1988, Allochthonous Archean basement in the northern East Humboldt Range, Nevada: Geology, v. 16, p. 349–353, doi: 10.1130/0091-7613(1988)016<0349:AABITN>2.3.CO;2.

McGrew, A.J., 1992, Tectonic evolution of the northern East Humboldt Range, Elko County, Nevada [Ph.D. thesis]: Laramie, University of Wyoming, 191 p.

McGrew, A.J., Peters, M.T., and Wright, J.E., 2000, Thermobarometric constraints on the tectonothermal evolution of the East Humboldt Range metamorphic core complex, Nevada: Geological Society of America Bulletin, v. 112, p. 45–60, doi: 10.1130/0016-7606(2000)112<0045:TCOTTE>2.3.CO;2.

Mueller, P.A., and Frost, C.D., 2006, The Wyoming Province: A distinctive Archean craton in Laurentian North America: Canadian Journal of Earth Sciences, v. 43, p. 1391–1397, doi: 10.1139/E06-075.

Nelson, S.T., Harris, R.A., Dorais, M.J., Heizler, M., Constenius, K.N., and Barnett, D.E., 2002, Basement complexes in the Wasatch fault, Utah, provide new limits on crustal accretion: Geology, v. 30, p. 831–834, doi: 10.1130/0091-7613(2002)030<0831:BCITWF>2.0.CO;2.

Pidgeon, R.T., Furfaro, D., Kennedy, A.K., Nemchin, A.A., and van Bronswjk, W., 1994, Calibration of zircon standards for the Curtin SHRIMP II, *in* Lanphere, M.A., et al., eds., Abstracts of the Eighth International Conference on Geochronology, Cosmochronology, and Isotope Geology: U.S. Geological Survey Circular 1107, p. 251.

Rodriguez, B.D., and Williams, J.M., 2008, Tracking the Archean-Proterozoic suture zone in the northeastern Great Basin, Nevada and Utah: Geosphere, v. 4, p. 315–328, doi: 10.1130/GES00120.1.

Sharp, R.P., 1942, Stratigraphy and structure of the southern Ruby Mountains, Nevada: Geological Society of America Bulletin, v. 53, p. 647–690.

Snoke, A.W., Hudec, M.R., Hurlow, H.A., and McGrew, A.J., 1990, The anatomy of a Tertiary extensional shear zone, Ruby Mountains–East Humboldt Range, Nevada: Geological Society of America Abstracts with Programs, v. 22, no. 3, p. 85.

Snoke, A.W., Howard, K.A., McGrew, A.J., Burton, B.R., Barnes, C.G., Peters, M.T., and Wright, J.E., 1997, The grand tour of the Ruby–East Humboldt metamorphic core complex, northeastern Nevada: Part 1—Introduction & Road Log, *in* Link, P.K., and Kowallis, B.J., eds., Proterozoic to recent stratigraphy, tectonics, and volcanology, Utah, Nevada, southern Idaho and central Mexico: Brigham Young University Geological Studies, v. 42 p. 225–269.

Strickland, A., Miller, E., and Wooden, J., 2007, SHRIMP-RG analyses of igneous and metamorphic minerals from the northern Grouse Creek Mountains, Utah: New evidence for the timing of Mesozoic and Cenozoic metamorphism and deformation: Geological Society of America Abstracts with Programs, v. 39, no. 6, p. 406.

Stroud, M.M., Foster, D.A., Mueller, P., Heatherington, A., Kamenov, G., and Wooden, J., 2007, The Farmington Canyon Complex: Implications for the evolution of the SW Laurentian Margin: Geological Society of America Abstracts with Programs, v. 39, no. 6, p. 221.

Tosdal, R.M., Cline, J.S., Hofstra, A.H., Peters, S.G., Wooden, J.L., and Young-Mitchell, M.N., 1998, Mixed sources of Pb in sedimentary-rock-hosted Au deposits, northern Nevada, *in* Tosdal, R.M., ed., Contributions to the gold metallogeny of northern Nevada: U.S. Geological Survey Open-File Report 98–338, p. 223–233.

Tosdal, R.M., Cline, J.S., Fanning, C.M., and Wooden, J.L., 2003, Lead in the Getchell–Turquoise Ridge Carlin-Type gold deposits from the perspective of potential igneous and sedimentary rock sources in northern Nevada: Implications for fluid and metal sources: Economic Geology and the Bulletin of the Society of Economic Geologists, v. 98, p. 1189–1211.

Vikre, P.G., 2000, Subjacent crustal sources of sulfur and lead in eastern Great Basin metal deposits: Geological Society of America Bulletin, v. 112, p. 764–782, doi: 10.1130/0016-7606(2000)112<0764:SCSOSA>2.3.CO;2.

Williams, I.S., 1997, U-Th-Pb geochronology by ion microprobe: Not just ages but histories: Economic Geology and the Bulletin of the Society of Economic Geologists, v. 7, p. 1–35.

Wooden, J.L., Kistler, R.W., and Tosdal, R.M., 1998, Pb isotopic mapping of crustal structure in the northern Great Basin and relationships to Au deposit trends, *in* Tosdal, R.M., ed., Contributions to the gold metallogeny of northern Nevada: U.S. Geological Survey Open-File Report 98–338, p. 20–33.

Wright, J.E., and Snoke, A.W., 1993, Tertiary magmatism and mylonitization in the Ruby–East Humboldt metamorphic core complex, northeastern Nevada: U-Pb geochronology and Sr, Nd, Pb isotope geochemistry: Geological Society of America Bulletin, v. 105, p. 935–952, doi: 10.1130/0016-7606(1993)105<0935:TMAMIT>2.3.CO;2.

Wright, J.E., and Wooden, J.L., 1991, New Sr, Nd, and Pb isotopic data from plutons in the northern Great Basin: Implications for crustal structure and granite petrogenesis in the hinterland of the Sevier thrust belt: Geology, v. 19, p. 457–460, doi: 10.1130/0091-7613(1991)019<0457:NSNAPI>2.3.CO;2.

Manuscript Received 19 November 2007
Revised Manuscript Received 3 May 2008
Manuscript Accepted 7 May 2008